

**A&A manuscript no.**  
 (will be inserted by hand later)  
**Your thesaurus codes are:**  
**03(11.17.1; 11.17.4 HE 1122-1649, HE 0515-4414; 11.01.1; 11.05.2; 11.09.4; 12.03.3)**

# Damped Lyman $\alpha$ systems at $z = 0.68$ and $z = 1.15$ towards HE 1122-1649 and HE 0515-4414 \*

**A. de la Varga<sup>1</sup>, D. Reimers<sup>1</sup>, D. Tytler<sup>2</sup>, T. Barlow<sup>3</sup>, and S. Burles<sup>4</sup>**

<sup>1</sup> Hamburger Sternwarte, Universität Hamburg, Gojenbergsweg 112, D-21029 Hamburg

<sup>2</sup> Center for Astrophysics and Space Sciences, University of California, San Diego, MS-0424, La Jolla, CA 92093-0424

<sup>3</sup> California Institute of Technology, 100-22, Pasadena, CA 91125

<sup>4</sup> Department of Astronomy and Astrophysics, University of Chicago, 5640 S. Ellis Ave., Chicago, IL 60637

Received date/ Accepted date

**Abstract.** Detailed analysis of the spectral lines from two low redshift damped Lyman alpha absorbers (DLA) confirms that they are a heterogeneous population. Both systems have low metal abundances of approximately 0.05 to 0.1 solar. The abundance pattern of the DLA at  $z = 1.15$  towards HE 0515-4414 shows dust depletion comparable to that found in our Galaxy, while the system at  $z = 0.68$  towards HE 1122-1649 shows abundance ratios resembling metal-poor halo stars with no dust depletion, for a comparable H I column. Constraints for N/Fe and N/Si also hint at  $z = 0.68$  DLA as a galaxy with recent star formation. The trend of increasing C I/H I with decreasing  $z$  is discussed. Only weak absorption from highly-ionized species associated with the DLA at moderate  $z$  have been detected and it probably originates in regions distinct from the low ionization gas. The low-ion profiles show very complex structures and are too large to be explained by the rotation of a disk: the system at  $z = 0.68$  spans over  $\sim 300$  km s $^{-1}$  and the  $z = 1.15$  DLA presents substructure over more than 700 km s $^{-1}$ , the largest velocity extent found up to date for a DLA.

**Key words:** Quasars: absorption lines – Quasars: individual: HE 1122-1649, HE 0515-4414  
 Galaxies: abundances – Galaxies: evolution – Galaxies: ISM – Cosmology: observations

---

*Send offprint requests to:* A. de la Varga

\* Based on observations performed at ESO/La Silla, on observations with the NASA/ESA Hubble Space Telescope and on observations at Keck Observatory.

*Correspondence to:* avarga@hs.uni-hamburg.de

## 1. Introduction

Damped Lyman  $\alpha$  absorbers (DLA) are the population of quasar absorption systems showing the highest neutral hydrogen column density ( $N(\text{H I}) \geq 2 \times 10^{20} \text{ cm}^{-2}$ ). At high redshift they contain the bulk of the cosmological mass of neutral gas in the Universe and are believed to be progenitors of current galaxies (e.g. Wolfe et al. 1986), although their nature and properties still remain unclear. They provide information about the chemical enrichment history of galaxies which can be contrasted with the studies of stellar populations in the local galaxies. Several samples of DLA at  $z > 1.7$  have been studied thoroughly (e.g. Pettini et al. 1990, Lu et al. 1996, Pettini et al. 1997a,b) but very few systems are known at intermediate or low redshift (Pettini & Bowen 1997, and references therein; Boissé et al. 1998, de la Varga & Reimers 1998, Pettini et al. 1999a,b). To interpret the high- $z$  data correctly, it is essential to follow the evolution of the DLA population to the present time. Moreover, at low  $z$  it is possible to search for luminous counterparts via imaging (e.g. Le Brun et al. 1997, Steidel et al. 1994, 1995, 1997, Rao & Turnshek 1998).

We herein present observations of two DLA, at  $z = 0.68$  and  $z = 1.15$ , in the line of sight to HE 1122–1649 and HE 0515–4414, respectively. The combination of HST spectra with high resolution spectra (CASPEC and HIRES) allows a detailed study of metal abundances and kinematics at low redshift.

Total metal abundances provide information about the population of absorbers which constitute DLA. Measurements of Zn and Cr show abundances of 1/15 solar, but with a considerable spread (Pettini et al. 1997b). The metallicity is not significantly higher for the few systems found at  $z < 1.5$  (Pettini et al. 1999a,b). The underabundance of Cr relative to Zn (Pettini et al. 1997a, 1999a,b) suggests that dust is also present, though the depletion level seems to be lower than in the Galaxy. The same conclusion was drawn from reddening studies of QSOs with and without DLA in their line of sight (e.g. Pei et al. 1991). The interplay between nucleosynthesis and dust depletion from the study of relative abundance patterns in DLA is still unclear (cf. Lu et al. 1996, Prochaska & Wolfe 1996, Pettini et al. 1997b, Kulkarni et al. 1997) and, however, crucial to understand the evolution and chemical enrichment of galaxies.

Studying the kinematics of the absorption line profiles should clarify the nature of DLA and could help to discern among theories of galaxy formation: are DLA related to rotating disks or rather to irregular protogalactic clumps merging, as expected in scenarios of hierarchical cosmogony? (cf. Prochaska & Wolfe 1997a,b, 1998, Haehnelt et al. 1998, McDonald & Miralda-Escudé submitted). Comparing profiles at low and high  $z$  could help to understand whether the asymmetries arise from a mixture of kinematical structures (random motions, rotation, infall, and merging...), or whether a trend can be recognized.

Our paper is organized as follows: in Sect. 2 we describe the observations and the data reduction. The analysis of the absorption lines is discussed in Sect. 3, the metal abundances in Sect. 4, and the relative abundances in Sect. 5. The neutral carbon and molecular content are studied in

Sects. 6 and 7, respectively. In Sect. 8 the kinematics of the absorption profiles is considered, and in Sect. 9 we study the highly-ionized gas related to the systems. Finally, concluding remarks are summarized in Sect. 10.

## 2. Observations and Data Reduction

### 2.1. HST Spectra

Ultraviolet spectra of HE 1122–1649 ( $z_{em} = 2.4$ , V=16.5, Reimers et al. 1995) were obtained with the Faint Object Spectrograph (FOS) onboard the Hubble Space Telescope (HST) in 1995. With gratings G270H and G190H (red digicon and entrance aperture of  $3.7'' \times 3.7''$ ), the wavelength range from 1600 to 3280 Å was covered with a maximum signal-to-noise ratio of 28. The spectral resolution is  $\text{FWHM} = 1.4$  and  $2.0$  Å for G190H and G270H, respectively (Schneider et al. 1993). The wavelength calibration of the pipeline reduced data was examined by comparing the overlap region between the G190H and the G270H spectra, and also with the Keck spectra, which have an overlap of 100 Å with the FOS spectra.

The spectra were corrected for interstellar reddening using the Seaton law (Seaton 1979) with  $E(B - V) = 0.08$ , corresponding to  $N(\text{H}1) = 4.16 \times 10^{20} \text{ cm}^{-2}$ . The high density of absorption lines complicates the measurement of a local continuum. Regions apparently free of absorption were selected by checking the error in the mean flux for consistency with the noise, and cubic splines were fitted to the mean flux values in those regions.

### 2.2. Keck HIRES Spectra

Optical data of HE 1122–1649 were taken with the HIRES spectrograph (Vogt et al. 1994) on the W.M. Keck1 10-m telescope with a total of 3 hours exposure in April 1997. The spectral range was from 3150 to 4710 Å with a S/N of 19/35 at 3500/4500 Å. We used a  $1.14'' \times 7.0''$  slit, which gave a resolution of  $8 \text{ km s}^{-1}$  FWHM ( $R=37500$ ) and adequate sky coverage, and used the UV cross-disperser to increase efficiency at wavelengths below 4200 Å. The images were processed and the spectra were optimally extracted using an automated package specifically designed by T. Barlow for HIRES spectra. Thorium-Argon lamp images were obtained immediately after the observations to provide wavelength calibrations in each echelle order. The root-mean-square residuals in the wavelength calibration for each echelle order were less than  $0.3 \text{ km s}^{-1}$ . All wavelengths are vacuum values in the heliocentric frame. Each echelle order was continuum fit with a Legendre polynomial to normalize the intrinsic QSO flux to unity.

### 2.3. CASPEC Spectra

Further optical spectra were obtained with CASPEC (Long Camera) at the 3.6 m telescope at ESO/La Silla. The data reduction was done with the ECHELLE software program available in

MIDAS, supplemented by software programmes for an optimal extraction of the echelle orders developed by S. Lopez. For wavelength calibration purposes, Th-Ar spectra were taken immediately before and after each quasar observation. The uncertainty in the calibration,  $\Delta\lambda$ , is given by the rms residuals after fitting third order polynomials to the lines identified in the arc lamp observations. For all the CASPEC observations we obtain  $\Delta\lambda \lesssim 0.2$  of a resolution element. The wavelength scales were corrected to vacuum-heliocentric values and individual observations re-binned to the same wavelength scale and combined by weighting by the inverse variance. The continuum for each echelle order was determined by iterative cubic spline fitting to regions free of absorption lines.

*HE 1122–1649 :*

In the observations of HE 1122–1649 in 1994, 43 echelle orders covered the wavelength range from 3750 to 5250 Å. The achieved resolving power, measured from the emission lines of the Th-Ar exposures, was  $R=17\,000$ , and the signal-to-noise ratio for the combined spectrum was 34, 43 and 53 at  $\lambda_{\text{obs}}=4000, 4500$  and 5000 Å, respectively. In 1996, 48 orders covered from 3320 to 4600 Å with S/N of 8/29 at 3500/4500 Å and  $R=20\,000$ .

*HE 0515–4414 :*

We observed HE 0515–4414 using CASPEC in October 1996 from 3530 to 4830 Å with  $R=21\,500$ , and 4865 to 6200 Å with  $R=24\,000$ . Further observations in November 1997 provided us with the ranges from 3250 to 4560 Å ( $R=27\,000$ ), 5430 to 7870 Å ( $R=28\,600$ ) and 6140 to 8570 Å ( $R=29\,000$ ). The combined spectrum covering the spectral range from 3250 to 8570 (with a small gap between 4830 and 4865 Å) has a maximum signal-to-noise ratio of  $\simeq 55$ .

### 3. Analysis of the Absorption Lines

Using the FITLYMAN program in the MIDAS package (Fontana & Ballester 1995), the absorption lines were fitted with Voigt profiles convolved with the instrumental profile, simultaneously determining the redshift, column density,  $b$  values and associated errors, while minimizing a  $\chi^2$  parameter matrix. Line parameters were taken from Morton (1991) and from Verner et al. (1994). Different transitions from the same ion were fitted simultaneously, and different ions and elements were fitted independently. We chose the minimum number of components which gave an adequate fit. Several fits were performed for the same complex by shifting slightly the initial  $z$  values and testing new sets. The considerable arbitrariness in the choice of components does not seriously affect the total column densities derived for most ions, as the presence of several transitions allow us to discern blends and hidden components –at least in the high resolution spectra– by means of the apparent optical depth method (Savage & Sembach 1991).

### 3.1. DLA at $z = 0.68$ towards HE 1122–1649

The profile of the damped Lyman  $\alpha$  is well fitted in the FOS spectrum by a column density of neutral hydrogen of  $\log N(\text{H}\text{I}) = 20.45 \pm 0.15$  at  $z = 0.6819$  (Fig. 1). A small correction for scattered light ( $\approx 1.5\%$  of the continuum) was applied to bring the core of the absorption line to zero flux.

We detect absorption at the expected position of numerous metal lines associated with this system. Table 1 lists the line parameters resulting from the fits, and Fig. 2 and 3 show some of the absorption features in velocity space.

We adopt  $3\sigma$  upper limits for lines which were not detected.

Comparable  $b$  values resulting from fits of individual components for different ions suggest that turbulent broadening is dominant. Under this assumption, for the cases where blending complicated the fitting, a typical  $b$  value was adopted as derived from the high resolution spectra for resolved lines. Keck spectra were filtered at the FOS instrumental resolution and new fits of the Fe II transitions longwards of Ly $\alpha$  were performed. We obtain  $b$  values of the order of  $\approx 30 \text{ km s}^{-1}$  by fitting the whole complex as a unique absorption feature at the resolution of the G270H spectra, and  $b \approx 25$  and  $16 \text{ km s}^{-1}$  fitting with two components at the resolution of G190H. Because of the severe blending in the Ly $\alpha$  forest, the line fits performed at the limited FOS resolution should be considered upper limits. However, the study on metal abundances will be based on column densities derived from the high resolution spectra.

The numerous Fe II transitions observed in the Keck spectra allow a reliable estimation of N(Fe) by fitting the strongest components in non-saturated transitions (Fe II 2260,2374). The best fit for Fe II requires at least 14 components (13 in the main feature plus the satellite component at  $v \simeq -100 \text{ km s}^{-1}$ ).

The non-detection of Zn II 2026 indicates that  $\log N(\text{Zn}) < 11.76$ . Several tests that modified the continuum level locally by means of fitting adjacent Ly $\alpha$  lines did not alter significantly the quoted value for the upper limit. Cr II transitions are blended with Ly $\alpha$  lines and with C IV at  $z = 1.234$ , so that an estimate of the column density for Cr II could not be derived. For the absorption feature between  $v \simeq 100$  and  $170 \text{ km s}^{-1}$ , Cr II 2062 yields an upper limit of  $\log N(\text{CrII}) \leq 12.2$  while  $\log N(\text{ZnII}) \leq 11.8$ . Ti II 1910.6,1910.9 are in a blended and noisy region of the spectrum, but recent Keck spectra (kindly provided by A. Songaila) covering up to 6060 Å allowed the detection of Ti II 3384 (at  $4\sigma$  level) at  $z = 0.6818927$  with  $\log N(\text{Ti II}) = 11.79 \pm 0.28$ ,  $b = 1.22 \pm 0.77$ .

### 3.2. DLA at $z = 1.15$ towards HE 0515–4414

According to IUE data, the extremely bright QSO HE 0515–4414 ( $z=1.7$ ,  $V=14.9$ , Reimers et al. 1998) has a DLA at  $z=1.15$  with an estimated column density for neutral hydrogen of  $\log N(\text{H}\text{I}) \simeq 20.4$ . We observe absorption associated with this sys-

tem at the expected positions of Al II 1670, Al III 1854,1862, C I 1656, C IV 1548,1550, Ca II 3934, Fe II 1608,2344,2374,2382,2586,2600, Mg I 1827,2026,2852, Mg II 2796,2803, Mn II 2576,2594,2606, Ni II 1741, Si II 1526,1808, Zn II 2026,2062. Upper limits for the column density of ions not detected over  $3\sigma$  are determined for Cr II 2056,2062, Fe I 2484, Na I 3303, S I 1807 and Ti II 3242. Figs. 4 and 5 show some of these ions in velocity space, and Table 3 the line parameters resulting from the fits. The line profiles of transitions of Mg II, Fe II and Al II reveal that this remarkably complex system extends over  $\sim 700 \text{ km s}^{-1}$ . At least three substructures can be distinguished: from approximately  $-575$  to  $-270 \text{ km s}^{-1}$ , from  $-260$  to  $-100 \text{ km s}^{-1}$  and the main absorption feature from  $-80$  to  $140 \text{ km s}^{-1}$ . Table 4 shows the derived column densities and metal abundances. The number of components is possibly underestimated because of the blending and blanketing problems. The  $b$  values resulting from the fit of a blend cannot be well determined, but the column density of a blend should be a good approximation of the column densities of individual lines, when the system is not heavily saturated (Jenkins 1986). The best fit for Mg II and Fe II requires at least 20 components for the whole system.

The main features in the Fe II complex were fitted on the weakest transitions (unsaturated), and the secondary ones on the strongest transitions (Fe II 2382,2600 were used for the absorption from  $-575$  to  $-270 \text{ km s}^{-1}$  and Fe II 2382,2600,2344 for the range  $-260$  to  $-100 \text{ km s}^{-1}$ ). Al II 1670 is saturated in the strongest substructure, and blended with Mg II at  $z = 0.2813$  in the secondary one. Al III 1862 is blended with Mg II 2803 at  $z = 0.4291$ .

A marginal  $2\sigma$  Ni II detection was obtained summing the spectral regions of Ni II 1741, Ni II 1709 and Ni II 1751 to improve the signal to noise ratio (stacking technique, e.g. Lu 1991). The upper limit for N(Cr) was derived in the same way.

### 3.3. Mg II System at $z = 0.28$ towards HE 0515–4414

The strong Mg II 2796 absorption features at  $z = 0.281$  reveal the presence of a multicomponent system spanning over  $\sim 200 \text{ km s}^{-1}$  from  $-40$  to  $175 \text{ km s}^{-1}$ , if  $v = 0 \text{ km s}^{-1}$  corresponds to  $z = 0.28135$  (Fig. 6). The corresponding Mg II 2803 lines could only be seen for the main structure (from  $-50$  to  $40 \text{ km s}^{-1}$ ), since the rest is blended with Al II 1670 at  $z = 1.15$ . The low redshift does not allow to identify many associated features in our optical data. Absorption lines at the expected positions of Fe II 2600, 2586, Fe I 3021, Mn II 2576,2606, Ca II 3969 and Al I 3803 have been looked for and the results of the fits are shown in Table 6. We obtain a Mn II /Fe II ratio about 15 times larger than solar, an improbable high value for a possible DLA. This suggests that the ionization is more complex, and/or that the continuum in the noisy region where Fe II is expected could be underestimated. Several tests considering higher local continua yield an upper limit of  $N(\text{Fe}) \leq 13.7$  which would mean an abundance of Mn relative to Fe five times larger than solar, if the Mn II 2576 feature is real. It remains unclear whether this system is

a new DLA candidate at very low redshift, maybe with an important part of Fe II depleted onto dust. Based on N(Mn II) and assuming a Mn abundance relative to H of 1/10 solar, we obtain  $\log N(\text{H I}) \simeq 19.9$ .

#### 4. Total Metal Abundances

In Table 2, 4 and 5 we show the total metal abundances derived assuming that H I dominates and, therefore, that ionization corrections are not important, as shown by ionization models (Lu et al. 1995, Viegas 1995).

Both DLA are metal-poor with values for the metallicity of 1/10 to 1/20 solar. These values are comparable to the abundances found in other DLA and confirm the results from previous studies (Lu et al. 1996, Pettini et al. 1997a,b, 1999a,b and references therein.):

(i) The large scatter in the metallicity of DLA at any redshift (1.6 in [Zn/H] over the whole range of  $z$ ) is consistent with the heterogeneous types of galaxies seen in the cases where the associated galaxy could be identified (e.g. Le Brun et al. 1997, Steidel et al. 1994, 1995, Rao & Turnshek 1998). Different star formation rates in spiral galaxies (Lindner et al. 1999), different impact parameters, and possible local inhomogeneities, would contribute to the scatter.

(ii) The enlarged sample shows no metallicity increase with decreasing  $z$ , contrary to expectations from models of cosmic chemical enrichment (e.g. Madau et al. 1996). Including the new values in the sample compiled from the literature, we obtain a column density-weighted mean abundance of Zn (Pettini et al. 1997a) of  $\langle [\text{Zn}/\text{H}] \rangle \leq -1.05$  at  $\langle z \rangle = 1$ , or  $\langle [\text{Zn}/\text{H}] \rangle_{\text{corr}} \leq -0.9$  if Zn is weakly depleted onto dust as in the Galaxy.

A bias in the observations against dust-rich absorbers could mean that the DLA found at low and moderate  $z$ , where the dust presence should be more important, are not representative galaxies (e.g. Boissé et al. 1998 and ref. therein). However, even considerable amounts of dust would not have been able to obscure the line of sight of the bright HE 0515–4414, and the intervening DLA still shows a rather low metallicity  $[\text{Zn}/\text{H}] \simeq -1$ . The upper limit of  $[\text{Zn}/\text{H}] < -1.3$  at  $z=0.68$ , obtained at the Keck resolution, is also noteworthy.

#### 5. Relative Metal Abundances

The ratio of two elements measured in DLA can vary from the solar value due to a different intrinsic pattern and/or to the condensation of refractory elements into dust depletion. We expect that the DLA might have abundance patterns resembling those in Halo stars, which show an overabundance of  $\alpha$ -group elements relative to Fe, and the odd-even effect (e.g. Mn underabundant relative to Fe.)

Assuming that elements in DLA are depleted as in the Galactic interstellar medium, Vladilo (1998) corrected the observed relative abundances from dust effects. He found the 17 systems of his sample chemically homogeneous over a range of metallicities from nearly solar down to

1/32 solar and the dust-corrected abundances remarkably close to the solar values. Applying the same correction to our systems, we obtain the dust-corrected abundances shown in Table 7.

Due to the probable heterogeneity of the DLA population, it is interesting to discuss the abundance pattern in the systems individually.

### 5.1. DLA at $z = 1.15$ towards HE 0515–4414: evidence for dust depletion

The refractory elements Cr, Ti, Ni are strongly depleted in this system:  $[\text{Cr}/\text{Zn}] < -1.04$ ,  $[\text{Ni}/\text{Zn}] < -1.19$ ,  $[\text{Fe}, \text{Ti}/\text{Zn}] < -0.66$ . These abundances are comparable with those observed in the warm disk and halo of our Galaxy (Savage & Sembach 1996). The *corrected* ratios are, in general, in line with those in Vladilo’s sample and consistent with solar. In particular,  $\alpha$  elements (e.g. Si, Ti) are not found to be overabundant relative to Fe, and Mn is not significantly underabundant relative to Fe-peak elements.<sup>1</sup>

The observed ratio  $\text{N}(\text{Ca II})/\text{N}(\text{Mg I})$  in this DLA, like in two DLA at  $z = 0.558, 0.5240$  (Vladilo et al. 1997 and references therein), is consistent with the predictions for warm gas with the base depletion representative of low density lines of sight in our Galaxy (Jenkins 1987). A selection bias would favour lines of sight with a base depletion pattern rather than a dense depletion, which would be present in gas with a smaller cross-section.

Recent observations of diffuse ISM along several lines of sight (Meyer et al. 1998 and ref. therein) show evidence for an ISM abundance of 2/3 solar, rather than solar, mainly based on measurements of O and Kr but also consistent with N, Zn, S and maybe C. We revised the correction for dust depletion in the abundance pattern of HE 0515–4414, assuming intrinsic abundances of 2/3 solar for all elements. The pattern remains almost unchanged, with deviations lower than 0.05 dex (mostly of  $\sim 0.02$  dex.)

The degree to which an element is depleted by dust grains in the Galactic ISM is known to anticorrelate roughly with the temperature at which half the atoms in the gas phase condense into solid form (e.g. Jenkins 1987). A trend suggesting a depletion pattern can be recognized for this DLA (Fig. 7), but it is mainly based on Zn, the only non-refractory element for which abundances could be determined.

### 5.2. DLA at $z = 0.68$ towards HE 1122–1649: no depletion pattern

The relative abundances observed in the DLA at  $z = 0.68$  (Table 2) differ considerably from solar, but follow a different pattern than the system at  $z = 1.15$ :

---

<sup>1</sup> The two Mn/Fe measurements from Vladilo (1998) yield  $[\text{Mn}/\text{Fe}]_{\text{corrected}} \simeq -0.2$  when adopting  $\log(\text{Mn}/\text{H})_{\odot} = -6.47$ , from Anders & Grevese (1989).

- The comparable Fe, Ti and Zn content in this system indicates that the effect of depletion onto dust is negligible, as expected at this low metallicity. Corrections for possible dust depletion are negligible.
- Mn is underabundant relative to Fe, as in the Galactic Halo, and  $[\text{Al}/\text{Si}] = -0.15 \pm 0.15$  is also compatible with the odd-even effect.
- The overabundance of  $\alpha$ -elements relative to Fe is observed for Si/Fe and compatible with the upper limit of O/Fe; however,  $[\text{Ti}/\text{Fe}] = -0.3 \pm 0.4$ .

Therefore, the abundance pattern shows similarities with metal-poor Halo stars. The low depletion degree could indicate that grain destruction is more efficient than in the Galaxy, maybe due to increased interstellar shocks from supernova explosions, as expected in a galaxy with intense star formation. Further abundance measurements of other weakly depleted elements (like S and O) would help to discern the intrinsic abundance pattern in DLA galaxies.

Plotting the measured abundances versus condensation temperature is consistent with the absence of a depletion pattern (Fig. 7). However, as argued by Pettini et al. (1997a), this lack of correlation should not be overinterpreted at such a low degree of chemical enrichment.

Other lines of sight in the enlarged  $z < 1.5$  DLA sample where the observed abundances could be corrected for depletion effects (Table 7), also show diverse patterns: e.g., low dust content is found at  $z = 0.8598$ ,  $z = 1.3726$ , and a pattern compatible with a solar one (or 2/3 of solar) for the corrected abundances at  $z = 1.223, 1.149, 1.42, 0.692$ . The different behaviours confirm that DLA arise in a heterogeneous group, as also inferred from the study of total abundances.

### 5.3. DLA Abundances and the Nucleosynthesis of Nitrogen

The Nitrogen abundance help us to decipher the Galactic chemical enrichment history. At low metallicities, N primary production, which takes place during the asymptotic giant branch phase of intermediate mass stars, is expected to dominate the secondary N production (e.g. Lu et al. 1998 and references therein). The time-delay between the production of primary N from intermediate mass stars and elements like O, released from massive stars, would imply a large scatter in N/O at low metal abundances (e.g. Marconi et al. 1994). However, observations of nearby metal-poor galaxies do not unambiguously show this pattern.

DLA offer the possibility of studying N abundances for metal-poor systems tracing early stages of the galactic chemical evolution and, therefore, of clarifying the N nucleosynthesis. DLA for which N abundances –or at least reliable upper limits– are available, are at high  $z$  (Pettini et al. 1995, Lu et al. 1998, Centurión et al. 1998 and references therein). The system at  $z = 0.68$  allows the first study of the N content at low redshift. In spite of the numerous N I transitions

expected in our spectral range, only upper limits could be derived for N(N I) due to the severe blending in the Ly $\alpha$  forest, yielding  $[N/H] < -2$ ,  $[N/Si] < -1.36$  and  $[N/Fe] < -0.64$ .

To compare with other systems, we assume that O and the  $\alpha$  elements (like S, Si) trace each other in DLA, as is the case in the Galaxy and in extragalactic H II regions. On the other hand, the lack of depletion onto galactic-like dust grains in this system implies that Fe and Si measurements correspond to the total elemental values, and therefore  $[N/O] \simeq [N/S] \simeq [N/Si]$  is assumed.

Lu et al. (1998) and Centurión et al. (1998) found that the N/Si, N/Fe and N/S ratios in a sample of DLA at high  $z$  show considerable scatter at low metallicities, as predicted by the standard model of delayed N primary production. The observed N/Fe for our DLA at  $z = 0.68$  is compatible with the range of measurements in Halo stars (cf. Figs. 6 and 7 in Centurión et al.). The low N/Si ( $\simeq$  N/O) limit agrees with the large dispersion and hints at a galaxy with recent star formation: O and Si have recently been released from massive stars and are overabundant relative to N, which has not had time to be primarily delivered from intermediate mass stars in significant amount and has not been secondarily produced in an efficient way at such a low metallicity level. The  $\alpha$ /Fe enhancement expected in a galaxy with a recent starburst is also observed in this system. On the contrary, Centurión et al. found no  $\alpha$  overabundance in the few DLA with low N/O values, and suggested that alternative models are required to explain those abundance patterns (e.g. primary N production in massive stars).

## 6. Neutral Carbon

Neutral species should be detectable in gas with a large H I column density. The detection of C I associated with DLA would be particularly interesting, since the ground-state fine-structure excitation depends on the cosmic microwave background radiation,  $T_{CMB}$ , and measuring the relative ground-state populations one can estimate the excitation temperature and an upper limit for  $T_{CMB}$  at that epoch (e.g. Ge et al. 1997 and references therein).

In Table 8 we compare the N(C I) measured in our systems with other values from the literature for a large range of  $z$ , and with those observed in Galactic lines of sight towards  $\zeta$  Oph (diffuses interstellar medium representative of the Galactic disk) and  $\zeta$  Pup (more tenuous inter-cloud medium and H II region). For the DLA at  $z = 1.15$ , the absorption features at the expected wavelength of C I 1656,1560 yield  $\log N(C I) = 13.68 \pm 0.09$  and  $\log N(C I^*) = 13.44 \pm 0.07$ . The relative population ratios imply an excitation temperature of 14.2 K, which is an upper limit to the  $T_{CMB}$ , since other mechanisms may contribute to the C I excitation (Lu et al. 1996). On the other hand, the complex structure of the  $z = 1.15$  DLA and the considerable noise in the C I 1560 region makes it difficult to deblend C I \* from further C I components. For the system at  $z = 0.68$ , we obtained an upper limit of  $\log N(C I) < 13.45$ .

Comparing these values with the C I/H I ratios known in Galactic gas (Jenkins & Shaya 1979) we find that the  $z = 1.15$  system reproduces the conditions of the Galaxy, as also found for a

DLA at  $z = 0.8597$  towards PKS 0454+039 (Boissé et al. 1998) and  $z = 1.97$  towards Q 0013-004 (Ge et al. 1997). The upper limit for the system at  $z = 0.68$  is still compatible with the conditions expected for Galactic gas but could also hint at a lower C I content as observed for a  $z = 0.692$  DLA towards 3C 286 (Boissé et al. 1998) and for the DLA at higher  $z$  in Table 8.

Plotting the C I/H I ratio versus redshift (Fig. 8), a trend of lower C I/H I with increasing  $z$  can be recognized. The overplotted linear regression is computed including upper limits as exact values. Considering that most of high  $z$  measurements are actually upper limits, the observed trend would be more pronounced. The evolution of the metagalactic ionizing background (more intense at high  $z$  than at  $z \lesssim 1$ , e.g. Haardt & Madau 1996) is probably the main reason of the C I/H I evolution with  $z$ . On the other hand, the local presence of dust could also be playing a role, since dust grains could shield more efficiently the gas from being photoionized. In fact, the DLA in Table 8 with a low dust content show a low C I/H I ratio, regardless of the redshift.

## 7. Molecules in DLA

We do not see (H<sub>2</sub>) or CO absorption, consistently with the low metal abundances.

Molecular hydrogen (H<sub>2</sub>) has numerous transitions at  $\lambda < 1100$  Å and carbon monoxide (CO) at  $\lambda < 1550$  Å. Because of the blending problem it is better to look for absorption-free windows where strong H<sub>2</sub> is expected than looking for strong lines themselves (Ge & Bechtold 1997). We do not find absorption at the expected positions of some strong H<sub>2</sub> lines (e.g. around  $\lambda_{rest} = 1094, 1079$ ) associated with the DLA at  $z = 0.68$ . The H<sub>2</sub>/H ratio is small compared to Galactic interstellar clouds, a common result for DLA (Ge & Bechtold, 1997). For the DLA at  $z = 1.15$ , the spectra do not cover the region where H<sub>2</sub> absorption is expected.

We searched for strong CO transitions ( $\lambda_{rest} = 1477.568, 1477.355, 1509.75, 1419.046, 1392.525, 1544.451$  Å) and obtained  $2\sigma$  upper limits of  $\log N(\text{CO}) < 14.4$  for the DLA at  $z = 0.68$  and  $\log N(\text{CO}) < 13.8$  at  $z = 1.15$  (where only  $\lambda_{rest} = 1544$  Å falls in the available wavelength range). Contrasting these values with the upper limits derived by Lu et al. (1998) at the Keck HIRES resolution for several DLA at high  $z$ , we find that our CO limits are roughly comparable to the values deduced for diffuse interstellar clouds in the Milky Way.

## 8. Kinematics: Complex Structure at Moderate $z$

The DLA at  $z = 0.68$  towards HE 1122–1649 extends over  $\sim 230$  km s<sup>-1</sup> in velocity space plus a satellite component at  $-100$  km s<sup>-1</sup>. As we can see in Figs. 2 and 3, the profiles of low ions observed at high resolution (cf. Fe II, Mg II, Mn II) track closely one another and show an edge-leading asymmetry, especially if we consider the feature from  $-20$  to  $100$  km s<sup>-1</sup>.

Remarkably, the Mg I 2852 profile shows a different asymmetry: the main feature lies between 100 and 150 km s<sup>-1</sup>, while Mg II – along with other singly ionized ions – shows the strongest absorption between  $\sim -20$  and 100 km s<sup>-1</sup>. This suggests that the region between

100 and 150  $\text{km s}^{-1}$  is less ionized, since the feature could not be identified as a metal line associated with another absorber. The difference between Mg I and Mg II profiles could hint at a non-negligible contribution of an intervening H II region for this system. The ionized gas would produce an extra contribution to the column densities of species with an ionization potential larger than 13.6 eV, so that the measured abundances of ions like Fe II, Mn II, Si II and Zn II would correspond to both regions. The metal abundances associated with the H I system would therefore be lower.

The low-ion profiles of the system at  $z = 1.15$  towards HE 0515–4414 (Figs. 4 and 5) span more than 700  $\text{km s}^{-1}$ , which is the largest extent in the velocity space seen for a DLA. As pointed out before, three main structures can be recognized: from approximately  $-575$  to  $-270$   $\text{km s}^{-1}$ , from  $-260$  to  $-100$   $\text{km s}^{-1}$  and the main absorber from  $-80$  to  $140$   $\text{km s}^{-1}$ . This main complex shows no ordered profile and is consistent with absorber components distributed randomly in  $v$ .

The remarkably complex structure of low and intermediate  $z$  DLA provide new hints about their nature. Two kinds of models have been discussed to explain kinematic characteristics of DLA at high  $z$ : (1) thick rotating disks evolving without merging to form present-day galaxies (Prochaska & Wolfe 1997a,b, 1998), and (2) merging protogalactic clumps in the standard Cold Dark Matter cosmology (Haehnelt et al. 1998, McDonald & Miralda-Escudé submitted). The model of rotating thick galactic disks can explain the edge-leading asymmetry of profile structures extending up to  $\sim 250$   $\text{km s}^{-1}$ . An asymmetric structure where the absorption decreases monotonously is found in the system at  $z = 0.68$ , but the one at  $z = 1.5$  shows a non-ordered profile. The large extent of the systems suggests that they cannot be single rotating disks.

Alternatively, several authors (e.g. Matteuci et al. 1997, Vladilo et al. 1997) have suggested that dwarf galaxies rather than spiral galaxies could be responsible for DLA. The extent of the kinematic profiles of our two new DLA are again too large to be explained by individual dwarf galaxies. On the other hand, Khersonsky & Turnshek (1996) showed that DLA can be associated with neutral gas in giant hydrogenous clouds that could be associated with any type of galaxy or protogalaxy.

Considering only the deepest part of the absorption ( $\tau \sim 0.7$ ) most profiles in a sample of high  $z$  DLA studied by Ledoux et al. (1998) show  $\Delta v < 150$   $\text{km s}^{-1}$  and a trend of decreasing velocity with increasing redshift. Under the same assumptions, our DLA at  $z = 0.68$  and  $1.15$  match fairly well this behaviour, which is expected in CDM structure formation scenario (e.g. Kauffmann 1996), but not if DLA are disks which do not evolve kinematically. Similarly to the models described by Haehnelt et al. 1998 for high  $z$ , the velocity broadening in the clumps at intermediate  $z$  would be due to a mixture of random motions, infall, merging and also rotation, which would still be important at smaller scales and could be responsible for the edge-leading asymmetry observed in some of the clumps.

Wolfe & Prochaska (1998) found a correlation between kinematics and metallicity for a sample of 17 DLA. At  $z = 1.6 - 3$  they detected no systems like our two, with a large extent in the velocity space ( $\Delta v > 120 \text{ km s}^{-1}$ ) and low metallicity ( $[\text{Zn}/\text{H}] \leq -1$ ) at the same time. On the other hand, the new systems do show moderate  $N(\text{H}\text{I})$  of  $\simeq 10^{20.4} \text{ cm}^{-2}$ , following the trend of larger  $\Delta v$  to lower  $N(\text{H}\text{I})$  observed for high redshift DLA (Wolfe & Prochaska 1998).

The ions associated with the DLA at  $z = 1.15$  towards HE 0515–4414 seem to track each other fairly well, but the lack of unsaturated lines from several ions at some velocities makes it difficult to establish the variation of the relative abundances. However, the strongest feature in the profiles of unsaturated Fe II and Mn II show two absorption features of comparable intensity, while for Zn II and Si II, the first one is clearly larger. Species weakly related to dust in the Galactic ISM seem to show a different profile than those corresponding to refractory elements. This could mean that there is more dust present in the components between  $-50$  and  $+50 \text{ km s}^{-1}$ , possibly associated with a higher metallicity level, and this dust could be partly concealing the edge-leading asymmetry.

## 9. Associated Highly-Ionized Gas.

Damped Ly $\alpha$  systems studied at high  $z$  often show considerable Si IV and C IV absorption with profiles resembling each other, but usually different from low ions (e.g. Lu et al. 1996). This suggests that highly-ionized gas is produced in distinct physical regions, which could be surrounding and shielding the low-ionized gas. In our two DLA at moderate redshift, we do not find strong lines from highly-ionized species covering a much larger extent than the weakly-ionized species.

- *DLA at  $z = 0.68$  towards HE 1122–1649:* Fig. 3 (right panel) shows absorption near the expected positions of C IV, O VI, Si III and Si IV, none of which is unambiguously present.
- *DLA at  $z = 1.15$  towards HE 0515–4414:* Only weak C IV absorption with  $N(\text{C IV}) = 13.18 \pm 0.12$  was found associated with the main complex at  $z = 1.15$  (from  $-80$  to  $140 \text{ km s}^{-1}$ ), contrary to most of DLA, but like  $z = 0.692$  towards 3C286 (Boissé et al. 1998), where no associated high ions could be found except for weak C IV. This suggests that the bulk of gas is weakly ionized and shielded from the ionizing radiation field. Stronger absorption features for the C IV doublet yielding  $N(\text{C IV}) = 14.38 \pm 0.17$  could be fitted in the noisy region extending from  $\sim -550$  to  $-200 \text{ km s}^{-1}$  (Fig. 4), which is less prominent in the low-ion profiles.

Al III measured in the DLA follows the low ionization species (Al III is observed for the three main substructures at  $z = 1.15$ ), but it is present in a much lower amount than Al II. These results confirm the very low ionization degree in these systems and suggest that Al III is probably produced in the same physical region as the low ionization species.

The absence of highly ionized gas associated with the large extents of low ionized regions suggests that the ionizing background is weaker than at high  $z$ , as expected from the cosmological expansion and from models of the ionizing background (e.g. Haardt & Madau 1996).

## 10. Summary

We have studied the properties of the DLA at  $z = 0.68$  towards HE 1122–1649 and at  $z = 1.15$  towards HE 0515–4414. A further DLA candidate at low redshift ( $z = 0.28$ ) has been found in the line of sight of HE 0515–4414. Very few DLA at  $z < 1.1$  had been analyzed up to now and enlarging the sample is essential to understand the nature of DLA, cosmic chemical evolution and possible selection effects which could be biasing our view of the Universe. The main results of our analysis, interpreted in comparison with DLA at other  $z$ , are summarized in this section:

- A large number of associated metal lines have been detected at high resolution. Metal abundances are found to be rather low (of 1/10 and  $< 1/20$  of solar value) and comparable to high- $z$  DLA. Therefore, the new values confirm the large scatter at any  $z$ , rather than a clear increase in the metallicity with decreasing  $z$  for the DLA population. The new systems also confirm the heterogeneity of the DLA population (in agreement with the results from imaging studies, e.g. by Le Brun et al. 1997).
- The relative abundance pattern for the DLA at  $z = 1.15$  in the line of sight of the very bright HE 0515–4414 indicates a significant degree of depletion, with a dust-to-metal ratio comparable to the Galactic value. The intrinsic pattern, after correcting for dust effects, is comparable to solar.
- The system at  $z = 0.68$  towards HE 1122–1649 presents a negligible dust content and its abundance pattern resembles that in metal-poor Halo stars. Relative abundances suggest that most metals in the  $z = 0.68$  DLA were made recently. Primary N production in massive stars is not required to explain the abundance pattern.
- The search for neutral carbon shows that systems without significant amounts of dust are not as shielded from ionizing sources as systems where dust is present. C I/H I increases with decreasing  $z$ , as expected from the evolution of the metagalactic ionizing background.
- The non-detection of H<sub>2</sub> or CO molecules is congruent with the low metal abundances.
- The high-resolution data reveal a very complex structure for the low-ion profiles. The system at  $z = 0.68$  spans over  $\sim 300$  km s<sup>−1</sup> and shows an edge-leading asymmetry. The  $z = 1.15$  system shows at least three main substructures over more than 700 km s<sup>−1</sup>. This suggests that the line of sight intersects a group of galaxies or subgalactic units. The velocity broadening could be due to a mixture of random motions, infall, merging and rotation.
- Only weak absorption from highly-ionized species were detected and it probably originates in regions distinct from the low-ionized gas.

Further surveys will provide new DLA candidates, which should be observed with the new echelle spectrographs and, at moderate redshift, also with imaging techniques in order to detect their galactic counterparts. Enlarging the DLA sample and clarifying their nature will help us to understand the cosmic chemical evolution and to discern among models of galaxy formation.

## References

Anders E., Grevesse N., 1989, *Geochim. Cosmochim. Acta* 53, 197

Blades J. C., Hustead R.W., Murdoch H.S., Pettini M., 1985, *ApJ* 288, 580

Boissé P., Le Brun V., Bergeron J., Deharveng J.M., 1998, *A&A* 333, 841

Centurión M., Bonifacio P., Molaro P., Vladilo G., 1998, *ApJ* 509, 620

Chaffee F.H., Foltz C.B., Black J.H., 1986, *Bull. AAS* 18, 1040

Chaffee F.H., Black J.H., Foltz C.B., 1988, *ApJ* 335, 584

Fontana A., Ballester P., 1995, *ESO Messenger* 80, 37

Ge J., Bechtold J., 1997, *ApJ* 477, L73

Ge J., Bechtold J., Black J.H., 1997, *ApJ* 474, 67

Haardt F., Madau P., 1996, *ApJ* 461, 20

Haehnelt M. G., Steinmetz M., Rauch M., 1998, *ApJ* , 495, 647

Jenkins E.B., 1986, *ApJ* 304, 739

Jenkins E.B., 1987, in *Interstellar Processes*, ed. D.J. Hollenbach, H.A. Thronson (Dordrecht: Reidel), 533

Jenkins E.B., Shaya E.J., 1979, *ApJ* 231, 55

Kauffmann G., 1996, *MNRAS* 281, 472

Kulkarni V.P., Fall S.M., Truran J.W., 1997, *ApJ* 484, L7

Khersonsky V. K., Turnshek D.A., 1996, *ApJ* 471, 657

Le Brun V., Bergeron J., Boissé P., Deharveng J. M., 1997, *A&A* 321, 733

Ledoux C., Petitjean P., Bergeron J., et al., 1998, *A&A* 337 L51

Lindner U., Fritze-von Alvensleben U., Fricke K.J., 1999, *A&A* 341, 709

Lu L., 1991, *ApJ* 379, 99

Lu L., Savage B.D., Tripp T.M., Meyer D., 1995, *ApJ* 447, 597

Lu L., Sargent W. L. W., Barlow T. A., Churchill C. W., Vogt S. S., 1996, *ApJS* 107, 475

Lu L., Sargent W. L. W., Barlow T. A., 1998, *AJ* 115, 55

Madau P., Ferguson H. C., Dickinson M. et al., 1996, *MNRAS* 283, 1388

Marconi G., Matteucci F., Tosi M. 1994, *MNRAS* 270, 35

Matteucci F., Molaro P., Vladilo V., 1997, *A&A* 321, 45

McDonald P., Miralda-Escudé J. 1999, *ApJ* 519, 486

Meyer D. M., York D. G., 1987a, *ApJ* 315, L5

Meyer D. M., York D. G., 1987b, *ApJ* 319, L45

Meyer D. M., York D. G. 1992, *ApJ* 399, L121

Meyer D. M., Black J.H., Chaffee F.H., Foltz C.B., York D. G., 1986, *ApJ* 308, L37

Meyer D.M., Lanzetta K.M., Wolfe A.M., 1995, *ApJ* 451, L13

Meyer D. M., Jura, M., Cardelli J.A., 1998, *ApJ* 493, 222

Morton D. C., 1978, *ApJ* , 222, 863

Morton D. C., 1991, *ApJS* 77, 119

Pei Y.C., Fall S.M., Bechtold J., 1991, *ApJ* 378, 6

Pettini M., Boksenberg A., Hunstead R. W., 1990, *ApJ* 348, 48

Pettini M., Lipman K., Hunstead R. W., 1995 *ApJ* 451, 100

Pettini M., Bowen D. V., 1997, *A&A* 327, 22

Pettini M., King D. L., Smith L. J., Hunstead R. W., 1997a, ApJ 478, 536

Pettini M., Smith L. J., King D. L., Hunstead R. W., 1997b, ApJ 486, 665

Pettini M., Ellison S.L., Steidel C.C., Bowen, D.V, 1999a, ApJ 510, 576

Pettini M., Ellison S.L., Steidel C.C., Shapley A. E., Bowen, D.V, 1999b, ApJ 532, 65

Prochaska J. X., Wolfe, A. M., 1996, ApJ 470, 403

Prochaska J. X., Wolfe A. M., 1997a, ApJ 474, 140

Prochaska J. X., Wolfe A. M., 1997b, ApJ 487, 73

Prochaska J. X., Wolfe A. M., 1998, ApJ 507, 113

Rao S.M., Turnshek D.A., 1998, ApJ 449, 488

Reimers D., Rodriguez-Pascual P., Hagen H.-J., Wisotzki L., 1995, A&A 293, L21

Reimers D., Hagen H.-J., Rodriguez-Pascual P., Wisotzki L., 1998, A&A 334, 96

Savage B. D., Sembach K. R., 1991, ApJ 379, 245

Savage B. D., Sembach, K. R., 1996, ApJ 470, 893

Schneider D. P., Hartig G.F., Januzzi B.T., et al., 1993, ApJS 87, 45

Seaton M.J. 1979, MNRAS 187, 73

Steidel C. C., Pettini M., Dickinson M., Persson S.E., 1994, AJ 108, 2046

Steidel C. C., Bowen D. V., Blades J. C., Dickinson M., 1995, ApJ 440, L45

Steidel C.C., Dickinson M., Meyer D.M., et al. 1997, ApJ 480, 568

de la Varga A., 1999, Ph.D.Thesis, University of Hamburg

de la Varga A., Reimers D., 1998, in Petitjean P., Charlot S. (eds.) Structure and Evolution of the intergalactic medium, Proc.IAP Col.1997, Frontiers, Paris

Verner D. A., Barthel P. D., Tytler D., 1994, AAPS 108, 287

Viegas S.M., 1995, MNRAS, 276, 268

Vladilo G., 1998, ApJ 493, 583

Vladilo G., Centurion M., Falomo R., Molaro P., 1997, A&A 327, 47

Vogt S. S., Allen A.L., Bigelow B.C., et al., 1994, Proc. SPIE, 2198, 362

Wolfe A. M., Prochaska J. X., 1998, ApJ 494, L15

Wolfe A. M., Turnshek D.A., Smith H.E., Cohen R.D., 1986, ApJS 61, 249

**Table 1.** Line fits in the DLA at  $z = 0.68$  towards HE 1122–1649

<i>Ion</i>	<i>z</i>	$\log N$	$\sigma_N$	<i>b</i>	$\sigma_b$
Al I	3083 0.6819088	12.17	0.07	10.0	0.0
Al II	1670 0.6820851	14.14	0.11	30.0	0.0
Al III	1862 0.6822000	$< 13.00$		30.0	0.0
C I	1656 0.6821087	$< 13.45$		30.0	0.0
C II	1334 0.6822630	18.30	0.29	30.0	0.0
Fe I	2523 0.6818900	$< 11.44$			
Fe II	2600 0.6813161	12.44	0.02	3.00	0.09
	2374 0.6818802	14.05	0.04	4.68	0.64
	2374 0.6819466	13.52	0.13	4.48	1.99
	2374 0.6820377	13.71	0.07	8.71	2.10
	2374 0.6821409	12.98	0.07	4.32	4.56
	2374 0.6822150	13.69	0.13	11.25	3.75
	2374 0.6823508	13.52	0.08	9.35	1.79
	2374 0.6824777	12.72	0.10	3.00	0.00
	2374 0.6825430	13.60	0.04	3.00	0.00
	2374 0.6825936	13.32	0.05	3.00	0.00
	2374 0.6826816	13.16	0.08	10.32	2.69
	2374 0.6828596	12.65	0.10	3.00	0.00
	2374 0.6829300	13.06	0.08	3.00	0.00
	2374 0.6830164	13.05	0.13	10.57	5.00
Mg I	2852 0.6819096	11.37	0.13	3.15	0.48
	2852 0.6821620	11.62	0.04	22.98	3.81
	2852 0.6825483	11.49	0.43	2.59	1.05
	2852 0.6826613	11.32	0.11	4.28	1.73
	2852 0.6829651	11.74	0.14	2.39	0.19
	2852 0.6832639	11.50	0.17	1.96	0.34
Mg II	2796 0.6813161	12.74	0.04	4.43	0.33
	2803 0.6813162	12.74	0.04	4.43	0.33
	2803 0.6818795	14.42	0.37	2.81	0.24
	2796 0.6818794	14.42	0.37	2.81	0.24
	2803 0.6819472	13.21	0.04	14.62	0.56
	2796 0.6819472	13.21	0.04	14.62	0.56
	2803 0.6820363	13.52	0.05	9.25	0.89

2796	0.6820364	13.52	0.05	9.25	0.89
2803	0.6821541	13.40	0.17	3.70	0.94
2796	0.6821541	13.40	0.17	3.70	0.94
2803	0.6822218	13.79	0.18	5.57	0.82
2796	0.6822218	13.79	0.18	5.57	0.82
2803	0.6823556	13.43	0.02	10.32	0.75
2796	0.6823556	13.43	0.02	10.32	0.75
2803	0.6824673	12.84	0.11	3.50	0.62
2796	0.6824672	12.84	0.11	3.50	0.62
2803	0.6825500	13.64	0.27	3.96	0.48
2796	0.6825500	13.64	0.27	3.96	0.48
2803	0.6826048	13.23	0.73	2.18	1.45
2796	0.6826049	13.23	0.73	2.18	1.45
2803	0.6826891	13.22	0.01	12.23	0.55
2796	0.6826891	13.22	0.01	12.23	0.55
2803	0.6828574	11.27	0.47	13.08	7.72
2796	0.6828575	11.27	0.47	13.08	7.72
2803	0.6829114	12.58	0.13	7.16	0.91
2796	0.6829112	12.58	0.13	7.16	0.91
2803	0.6829443	12.25	0.27	2.30	0.71
2796	0.6829442	12.25	0.27	2.30	0.71
Mn I	2799	0.6818900	< 11.67		
Mn II	2576	0.6818700	11.68	0.09	2.93
	2594	0.6818699	11.68	0.09	2.93
	2576	0.6819273	11.55	0.11	1.55
	2594	0.6819273	11.55	0.11	1.55
N I	1199	0.6818900	< 14.5	30.0	0.00
N V	1238	0.6818900	< 14.0		
			1242		
Ni I	2346	0.6818900	< 12.07		
Ni II	1317	0.6818900	< 13.65		
O I	1039	0.681890	< 17.00	30.0	0.00
O VI	1031	0.6821704	18.94	0.09	0.00
S I	1807	0.6820000	< 14.05		
S III	1012	0.6820000	< 14.99		

Si I	2515	0.6818900	< 14.58				
Si II	1193	0.6819438	15.32	0.09	25.00	0.00	
	1190	0.6819438	15.32	0.09	25.00	0.00	
	1193	0.6825498	14.36	0.12	16.00	0.00	
	1190	0.6825498	14.36	0.12	16.00	0.00	
Si IV	1402	0.6823700	14.32	0.23	30.	0.0	
Ti II	3384	0.6818927	11.70	0.28	1.19	0.7	
Zn I	2139	0.68189	< 11.28				
Zn II	2026	0.68189	< 11.76				

**Table 2.** Metal abundances of the DLA at  $z = 0.68$  with  $\log N(\text{H}\text{I}) = 20.45 \pm 0.15$ . We adopt the classical definition  $[\text{X/Y}] \equiv \log (\text{X/Y})_{\text{obs}} - \log (\text{X/Y})_{\odot}$ , where solar values are taken from Anders & Grevesse (1989).

Element	$\log N(\text{cm}^{-2})$	Total Abundance	[Metal/Fe]	[Metal/Zn]
Al	$14.14 \pm 0.11$	$-0.79 \pm 0.12$	0.57	$> 0.55$
C	$18.30 \pm 0.29$	$1.28 \pm 0.29$	2.64	$> 2.62$
Fe	$14.60 \pm 0.28$	$-1.36 \pm 0.28$		$> -0.02$
Mg	$> 14.71$	$> -1.32$	$> 0.04$	
Mn	$11.92 \pm 0.14$	$-2.06 \pm 0.15$	-0.7	$> -1.02$
N	$< 14.5$	$< -2.$	$< -0.64$	
Ni	$< 13.65$	$< -1.05$	$< 0.31$	
O	$< 17$	$< -0.38$	$< 0.98$	
Si	$15.36 \pm 0.12$	$-0.64 \pm 0.13$	0.72	
Ti	$11.70 \pm 0.28$	$-1.68 \pm 0.28$	-0.32	$> -0.34$
Zn	$< 11.76$	$< -1.34$	$< 0.02$	

**Table 3.** Line fits in the DLA at  $z = 1.15$ .

<i>Ion</i>	<i>z</i>	$\log N$	$\sigma_N$	<i>b</i>	$\sigma_b$
Al II	1670	1.1468446	11.44	0.19	7.03
		1.1469733	12.40	0.20	2.77
		1.1470984	11.80	0.20	2.37
		1.1472185	12.08	0.19	8.80
		1.1475825	12.01	0.06	1.43
		1.1480030	11.36	0.10	9.38
		1.1484466	11.98	0.08	1.26
		1.1487808	12.53	0.45	0.21
		1.1490958	13.02	0.38	2.85
		1.1495245	11.80	0.08	7.67
		1.1498086	12.69	0.08	1.07
		1.1507328	12.13	1.09	23.51
		1.1508443	15.42	0.87	7.71
		1.1511260	12.64	0.15	9.91
		1.1512798	13.53	0.82	5.13
		1.1513751	12.05	0.77	25.35
Al III	1854	1.1490991	11.88	0.06	2.84
	1862			1.30	
	1854	1.1508672	12.07	0.07	14.73
C I	1656	1.1508082	13.56	0.04	9.31
	1560	1.1508083			
	1656	1.1513586	13.05	0.09	12.68
	1560	1.1513586			
C I *	1656.21.1507983	13.44	0.07	7.48	2.45
C I *	1657.91.1507983				
C IV	1548	1.1471568	13.63	0.06	20.69
	1550	1.1471567	13.63	0.06	20.69
	1548	1.1475769	13.55	0.08	9.33
	1550	1.1475769	13.55	0.08	9.33
	1548	1.1480157	13.68	0.08	7.03
	1550	1.1480159	13.68	0.08	7.03
	1548	1.1482468	13.74	0.07	10.06
	1550	1.1482468	13.74	0.07	10.06

	1548	1.1485275	13.61	0.08	24.69	5.03
	1550	1.1485275	13.61	0.08	24.69	5.03
	1548	1.1491662	13.26	0.09	11.06	3.27
	1550	1.1491662	13.26	0.09	11.06	3.27
C IV	1548	1.1508356	13.18	0.12	10.12	4.35
	1550					
Ca II	3934	1.1508502	11.87	0.23	7.23	4.79
		1.1509476	12.17	0.14	30.14	8.88
		1.1513215	12.25	0.05	12.60	1.82
Cr II	2056	1.150800	< 12.10			
Fe I	2484	1.150800	< 11.57			
Fe II	2600	1.1469649	12.43	0.05	2.30	0.51
		1.1469650	12.43	0.05	2.30	0.51
		1.1471601	11.93	0.15	10.52	2.81
		1.1471599	11.93	0.15	10.52	2.81
		1.1472481	12.66	0.05	50.32	5.67
		1.1472480	12.66	0.05	50.32	5.67
		1.1479497	12.58	0.03	21.17	1.63
		1.1479497	12.58	0.03	21.17	1.63
		1.1490909	13.11	0.13	2.40	0.21
		1.1490909	13.11	0.13	2.40	0.21
		1.1495110	12.54	0.02	8.42	0.78
		1.1495110	12.54	0.02	8.42	0.78
		1.1498045	12.21	0.06	4.82	3.59
		1.1498046	12.21	0.06	4.82	3.59
		1.1499078	12.06	0.10	2.89	1.22
		1.1499077	12.06	0.10	2.89	1.22
	2374	1.1508005	13.75	0.01	9.54	0.64
		1.1509480	13.68	0.05	1.73	0.12
		1.1510571	13.13	0.06	2.30	0.62
		1.1512597	13.64	0.03	15.35	1.27
		1.1512957	13.18	0.18	1.01	6.68
Mg I	1827	1.1508058	12.86	0.09	16.34	4.68
	2026					
	2852	1.1508093	12.06	0.02	7.19	0.52

	1.1509610	12.29	0.02	29.61	1.07	
	1.1513028	11.95	0.02	11.32	0.54	
Mg II	2796	1.1469659	12.79	0.23	2.88	1.04
	2803	1.1469659	12.79	0.23	2.88	1.04
	2796	1.1470861	13.00	0.05	28.34	2.83
	2803	1.1470863	13.00	0.05	28.34	2.83
	2796	1.1471353	12.34	0.08	4.53	2.01
	2803	1.1471351	12.34	0.08	4.53	2.01
	2796	1.1472504	12.29	0.16	5.40	2.42
	2803	1.1472507	12.29	0.16	5.40	2.42
	2796	1.1474081	12.11	0.11	5.15	1.77
	2803	1.1474082	12.11	0.11	5.15	1.77
	2796	1.1475828	12.25	0.02	7.17	0.60
	2803	1.1475830	12.25	0.02	7.17	0.60
	2796	1.1479594	12.62	0.01	26.94	0.91
	2803	1.1479595	12.62	0.01	26.94	0.91
	2796	1.1485009	12.34	0.02	20.98	1.22
	2803	1.1485010	12.34	0.02	20.98	1.22
	2796	1.1491084	12.85	0.01	9.75	0.19
	2796	1.1495093	12.34	0.03	7.06	0.63
	2796	1.1496212	12.43	0.05	34.58	5.65
	2796	1.1498080	12.77	0.55	2.10	0.51
	2796	1.1499032	12.21	0.08	6.85	1.32
	2803	1.1503466	11.65	0.16	6.43	3.15
	2803	1.1506114	12.79	0.11	21.11	3.89
	2803	1.1508448	13.80	0.04	15.89	0.87
	2803	1.1509888	13.41	0.12	23.32	4.36
	2803	1.1512514	13.41	0.08	31.96	1.92
	2803	1.1512749	15.11	0.42	4.94	0.49
	2803	1.1517754	11.74	0.11	9.73	4.27
Mn II	2576	1.1507992	11.67	0.08	4.61	2.30
	2594	1.1507992	11.67	0.08	4.61	2.30
	2606	1.1507992	11.67	0.08	4.61	2.30
Mn II	2576	1.1512835	11.58	0.11	4.09	5.22
Na I	3303	1.1508000	< 12.9			

Ni II	1741	1.1507868	< 12.52	0.12	5.19	3.94
S I	1807	1.1508000	< 12.52			
Si II	1808	1.1507919	14.51	0.05	7.2	2.8
Si II	1526					
Si II	1808	1.1509281	13.98	0.14	2.08	4.19
Si II	1526					
Si II	1808	1.1512949	14.12	0.11	2.49	3.19
Si II	1526					
Zn II	2026	1.1513157	12.11	0.04	9.15	1.66

**Table 4.** Metal column densities and total abundances for the DLA at  $z = 1.15$  adopting  $\log N(\text{H}1) = 20.45$ . Feature I, II and III correspond to the substructures from  $-575$  to  $-270$ , from  $-260$  to  $-100$  and from  $-80$  to  $140 \text{ km s}^{-1}$ , respectively.

<i>Total Abundance</i>	$N_{\text{Feature}I}$	$N_{\text{Feature}II}$	$N_{\text{Feature}III}$
$[\text{Al}/\text{H}] \geq 0.5$	$13.01 \pm 0.61$	$13.20 \pm 0.40$	$\geq 15.4$
$[\text{Ca}/\text{H}] > -2.19$			$12.60 \pm 0.27$
$[\text{Cr}/\text{H}] \leq -2.03$			
$[\text{Fe}/\text{H}] = -1.65$	$13.08 \pm 0.17$	$13.28 \pm 0.17$	$14.24 \pm 0.20$
$[\text{Mg}/\text{H}] \geq -0.8$	$13.47 \pm 0.22$	$13.29 \pm 0.56$	$\geq 15.15$
$[\text{Mn}/\text{H}] = -2.05$		$< 11.4$	$11.93 \pm 0.11$
$[\text{Ni}/\text{H}] < -2.18$			$< 12.52$
$[\text{Si}/\text{H}] = -1.26$		$< 13.8$	$14.74 \pm 0.18$
$[\text{Ti}/\text{H}] \leq -1.65$			$< 11.7$
$[\text{Zn}/\text{H}] = -0.99$		$< 11.5$	$12.11 \pm 0.04$

**Table 5.** Relative Metal abundances for the DLA at  $z = 1.15$ .

Element	$[X/Fe]_{Total}$	$[X/Fe]_{Main}$	$[X/Zn]_{Total}$
Al	> 2.12	> 2.19	> 1.46
Ca II	-0.54	-0.47	-1.2
Cr	< -0.38	< -0.31	< -1.04
Fe			-0.66
Mn	-0.40	-0.59	-1.06
Ni	< -0.53	< -0.46	< -1.19
Si	0.39	0.46	-0.27
Ti	< -0.03	< -0.07	< -0.66
Zn	0.66	0.73	

**Table 6.** Line parameters for the absorber at  $z = 0.28$  towards HE 0515–4414

	<i>Ion</i>	<i>z</i>	$\log N(\text{cm}^{-2})$	$\sigma_N$	<i>b</i> ( $\text{km s}^{-1}$ )	$\sigma_b$
Al I	3969	0.2813500	< 11.91			
Ca II	3969	0.2813500	< 11.57			
Fe I	3021	0.2813500	< 12.12			
Fe II	2600	0.2813753	13.14	0.09	15.00	0.00
	2600	0.2817716	12.96	0.20	5.29	4.82
Mn II	2576	0.2813256	12.46	0.15	8.00	0.00
	2606	0.2813256	12.46	0.15	8.00	0.00
Mg II	2796	0.2812490	12.44	0.08	13.93	3.54
	2803	0.2812490	12.44	0.08	13.93	3.54
	2796	0.2813520	12.77	0.27	6.92	2.42
	2803	0.2813521	12.77	0.27	6.92	2.42
	2796	0.2814065	12.73	0.30	13.52	4.79
	2803	0.2814064	12.73	0.30	13.52	4.79
	2796	0.2817727	14.13	0.26	4.82	0.35
	2796	0.2818092	12.61	0.09	15.93	2.74
	2796	0.2819882	13.44	1.57	2.62	0.67
	2796	0.2820545	12.19	0.07	4.89	2.55

**Table 7.** Relative ratios for a sample of DLA at  $z < 1.5$ . For each system, the observed ratios are shown in the first row, and the ratios corrected for dust depletion are given in the second row.

$z_{DLA}$	QSO	[Zn/Cr]	[Zn/Fe]	[Si/Fe]	[Ti/Fe]	[Mn/Fe]	[Ni/Fe]	[Cr/Fe]	[S/Fe]	Ref.*
1.15	HE 0515–4414	> 1.04	0.66	0.39	0.00	-0.40	<-0.53	<-0.38	1	
		> 0.05	0.00	-0.03	-0.01	-0.07	<-0.03	<-0.05		
0.68	HE 1122–1649		<0.02	0.72	-0.32	-0.70	<0.31		1	
			<0.00	0.69	-0.29	-0.60	<0.29			
0.3953	PKS1229–0210	> 0.35	> 0.85	> 0.56		> 0.49	> 0.02		2	
		>-0.10	> 0.24	> 0.11		> 0.14	> 0.01			
0.6560	3C336		< 1.04			<-0.29			3	
			< 0.00			<-0.04				
0.6920	3C286	0.50	0.71			<-0.29	< 0.46	0.21	4,2	
		-0.05	0.07			<-0.06	< 0.01	0.04		
0.8598	PKS0454+0356	0.07	-0.07			-0.36	-0.57	-0.14	5	
		0.08	-0.06			-0.38	-0.63	-0.15		
1.0095	EX 0302–233	0.39	< 0.89				< 0.50	<0.50	6,2	
		-0.10	< 0.24				< 0.15	< 0.14		
1.1491	Q 1351+318	0.57	0.64	0.45		-0.16	<-0.41	0.07	9	
		0.00	0.01	0.00		-0.05	<-0.03	0.00		
1.2232	Q 1247+267	0.20	0.37	0.28		-0.19	< -0.48	0.17	9	
		-0.05	0.07	0.07		-0.09	< -0.13	0.07		
1.3726	Q 0935+417	0.10	0.29			-0.39		0.19	7,8	
		-0.06	0.09			-0.19		0.11		
1.4200	Q 1354+258	0.20	0.42	0.30		-0.29	-0.65	0.22	9	
		-0.06	0.10	0.07		-0.11	-0.15	0.10		

\* (1) This work, (2) Boissé et al. 1998, and ref. therein, (3) Steidel et al. 1997, (4) Meyer & York 1992, (5)

Lu et al. 1996, (6) Pettini & Bowen 1997, (7) Meyer, Lanzetta & Wolfe 1995, (8) Pettini et al. 1997a, and

(9) Pettini et al. 1999.

**Table 8.** C I measurements in DLAs and in the Galaxy.

Sightline	$z$	$\log N(HI)$	$\log N(CI)$	$[Zn/H]$	References*
2000-330	3.19	19.69	< 12.90		1
0741+4741	3.02	20.03	< 12.12	< -0.79	8
0528-250	2.81	21.28	< 13.48	-0.76	2
0201+365	2.46	20.8	13.23	> 0.56	3
2243-6031	2.33	20.39	< 12.55	-1.06	8
PHL 957	2.31	21.40	< 12.65		4
0013-004	1.97	20.70	13.65		5
1331+170	1.78	21.18	13.28	-1.27	6
0215+015	1.35	19.80	13.90		7
0515-4414	1.15	20.45	13.68	-0.99	11
0454+039	0.86	20.69	13.64	-0.8	9
3C286	0.69	21.25	13.57	-1.1	9
1122-1649	0.68	20.45	< 13.45	< -1.3	11
$\zeta$ Orp	0	21.15	15.34		10
$\zeta$ Pup	0	20.0	12.80		10

\*(1)Meyer & York 1987a, (2)Meyer & York 1987b and ref. therein, (3) Prochaska & Wolfe 1996, (4)Meyer et al. 1986, Chaffee et al. 1986, (5) Ge et al. 1997, (6) Chaffee et al. 1988 and ref, therein, (7) Blades et al. 1985, (8) de la Varga 1999, (9) Boissé et al. 1998 (10) Morton 1978, (11) This paper.

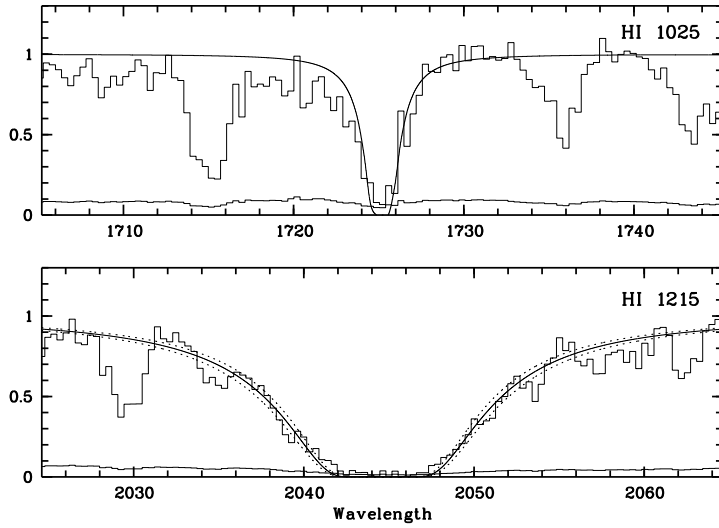


**Fig. 1.** HI Ly $\alpha$ , Ly $\beta$  and Ly $\gamma$  for the damped Lyman  $\alpha$  system at  $z = 0.6819$  towards HE 1122–1649. The best fit is found for  $\log N(\text{HI}) = 20.45 \pm 0.15$  fitting Ly $\alpha$  and Ly $\beta$  simultaneously (Ly $\gamma$  was not used, since it lies on a too noisy and blended region).

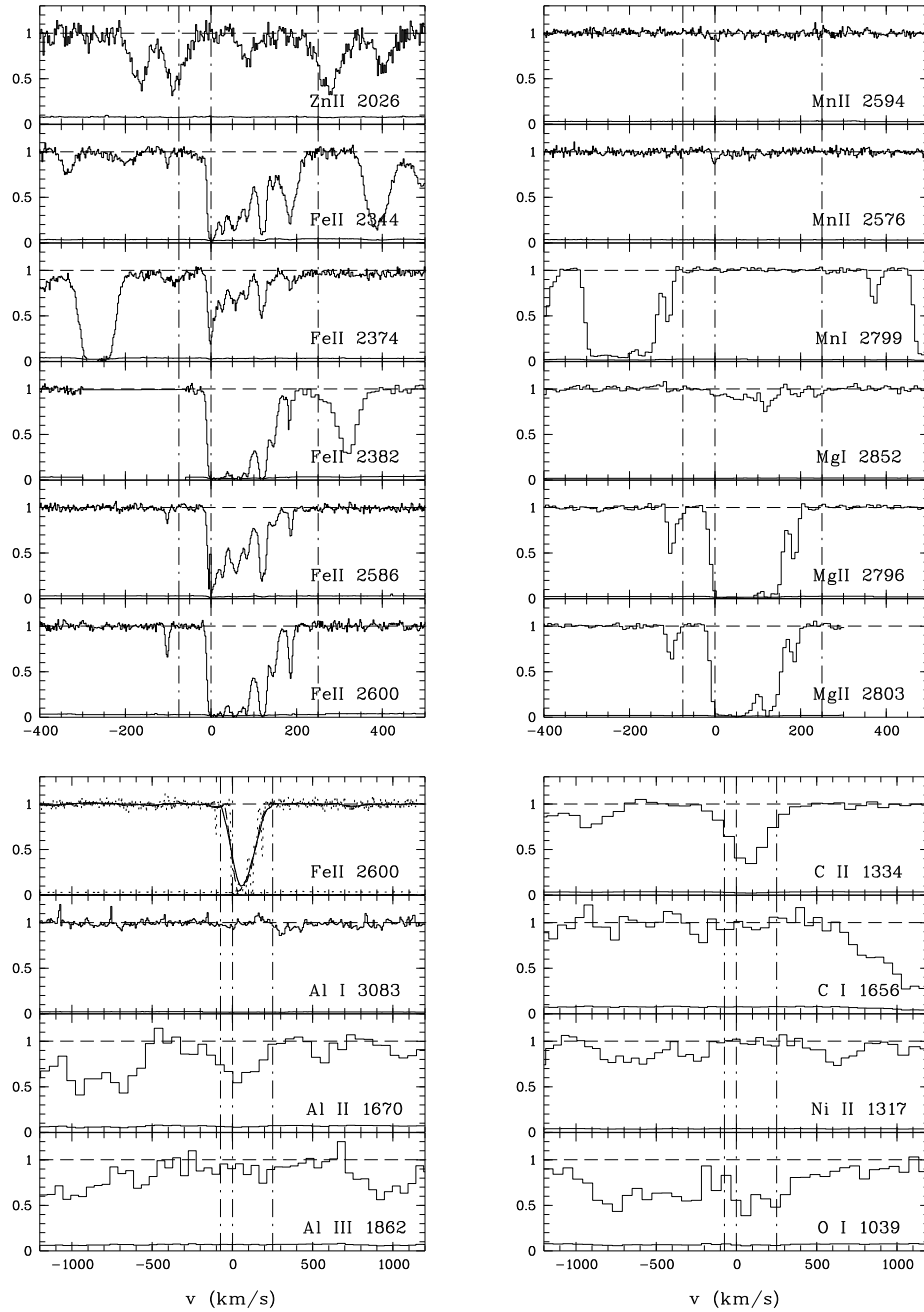


**Fig. 2.** Velocity profiles of some ions associated with the DLA at  $z = 0.68$  towards HE 1122–1649 ( $v = 0 \text{ km s}^{-1}$  corresponds to  $z = 0.68189$ ). The solid line overplotted for the ion Fe II 2600 in the bottom-left panel shows the absorption profile as it would be seen at the HST/FOS resolution (compare with Fe II 2600 at Keck/HIRES resolution in upper-left panel)

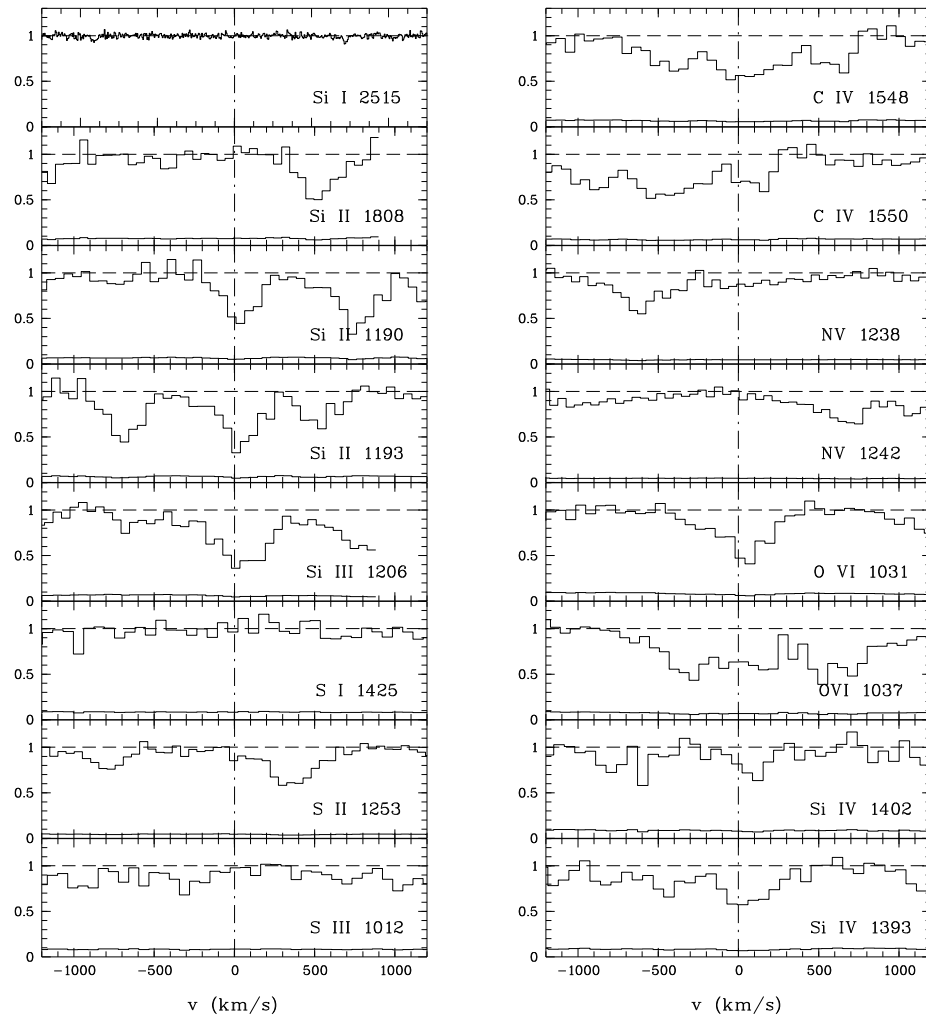


**Fig. 3.** (...) Velocity profiles of some ions associated with the DLA at  $z = 0.68$  towards HE 1122–1649 ( $v = 0 \text{ km s}^{-1}$  corresponds to  $z = 0.68189$ ).

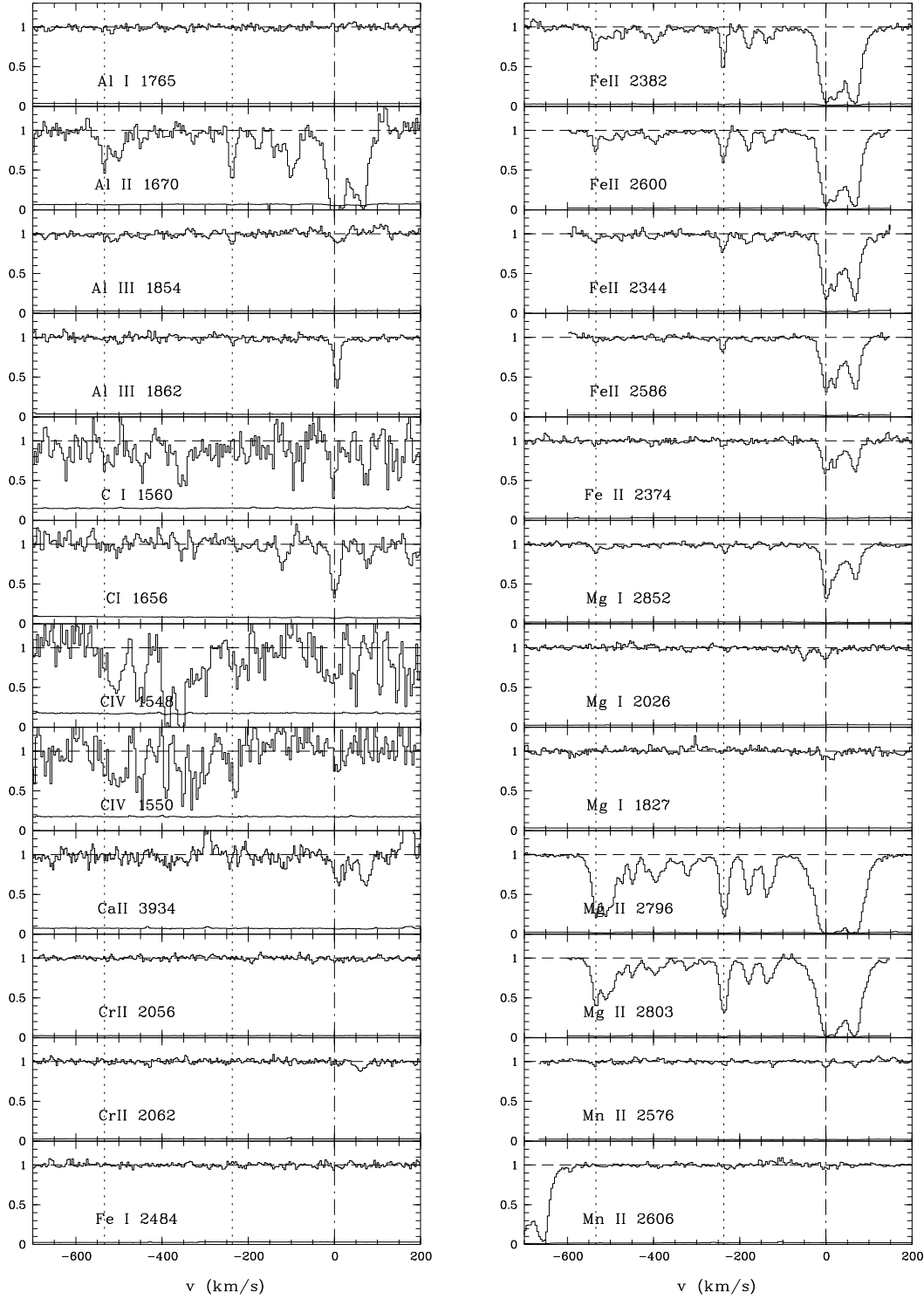


**Fig. 4.** Velocity profiles of some ions associated with the DLA at  $z = 1.15$  towards HE 0515–4414 ( $v = 0 \text{ km s}^{-1}$  corresponds to  $z = 1.15080$ ).

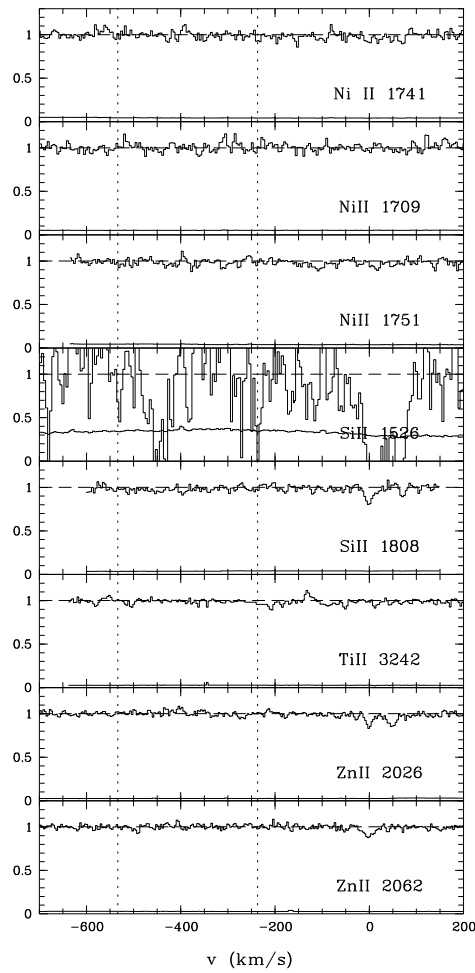


**Fig. 5.** (...)Velocity profiles of some ions associated with the DLA at  $z = 1.15$  towards HE 0515–4414 ( $v = 0 \text{ km s}^{-1}$  corresponds to  $z = 1.15080$ ).

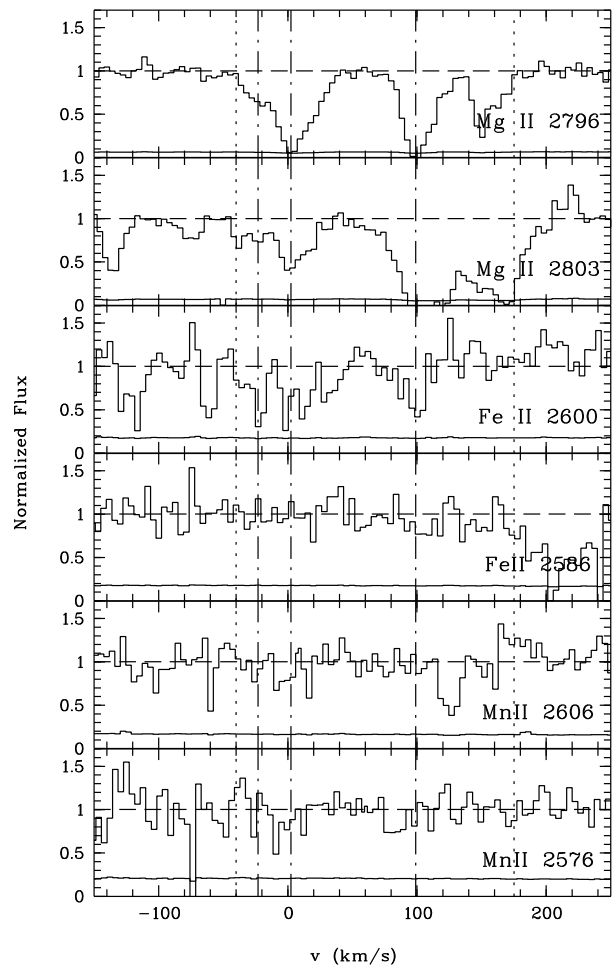


**Fig. 6.** Velocity profiles of ions associated with the Mg II system at  $z = 0.28135$  (corresponds to  $v = 0 \text{ km s}^{-1}$ ) towards HE 0515–4414 .

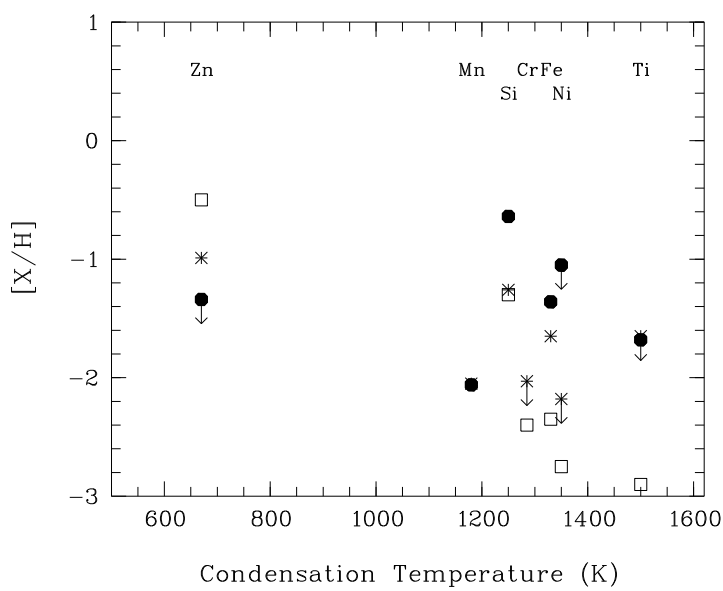


**Fig. 7.** Some metal abundances versus condensation temperature for the  $z = 0.68$  system (filled circles), the  $z = 1.15$  system (asterisks) and in the ISM line of sight towards  $\zeta$  Oph from Savage & Sembach 1996 (open squares).

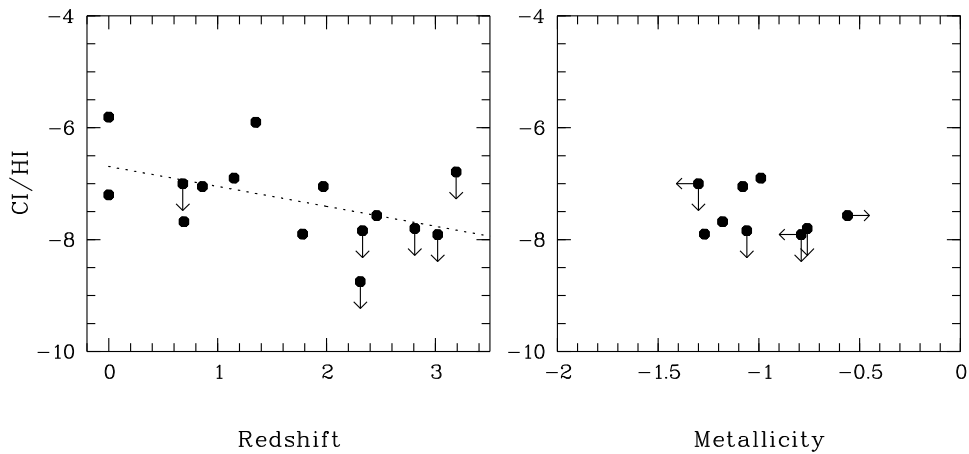


**Fig. 8.** Evolution of the  $\text{C I}/\text{H I}$  ratio with redshift (left panel), and with the metallicity (right panel) References are given in Table 8.